PROCEEDINGS OF SCIENCE

Generalized Parton Distributions program at COMPASS

Eric Fuchey* **(on behalf of COMPASS collaboration)**
CEA Saclay
E-mail: eric.fuchey@cea.fr

Understanding the structure of the nucleon remains one of the key challenges of nuclear physics. Yet, there are many open questions concerning the nucleon structure: For instance, the total spin of the proton cannot be explained by the sum of the spins of the quarks it contains; this is called the proton spin puzzle. The Generalized Parton Distributions (GPDs) grant a new insight on the study of the nucleon structure, as they provide a three-dimensional picture of the nucleon. They may also grant access to quark orbital angular momentum, which is one of the possible keys to solve the proton spin puzzle. COMPASS at CERN has a great potential for GPD studies, with its forthcoming measurement of deeply virtual Compton scattering and exclusive meson production off the proton with both polarized μ^+ and μ^-. The current COMPASS GPD program will be discussed. Existing results of DVCS and exclusive meson production will be presented. An overview of the investigation on future possible developments will briefly be introduced.

QCD Evolution 2015,
26-30 May 2015
Jefferson Lab (JLAB), Newport News Virginia, USA

*Speaker.

PoS(QCDEV2015)048

1. Reminder on Generalized Parton Distributions

The Generalized Parton Distributions (GPDs) constitute a new, three dimensional parametrization of the nucleon structure. They correlate the momentum distribution of the partons inside the proton, parametrized by the parton distribution functions, to the transverse spatial distribution of those partons, parametrized by the form factors. As such, those objects grant access to the orbital angular momentum of the quarks [1, 2, 3].

GPDs can be accessed thanks to exclusive processes such as Deeply Virtual Compton Scattering (DVCS $\ell p \to \ell p \gamma$), or exclusive meson production off the nucleon. In such reactions, the virtual photon (with a high virtuality Q^2) emitted by the lepton selects a quark in the nucleon with a longitudinal momentum fraction $x+\xi$, which emits a real photon (in the case of DVCS) or produces a meson (in the case of meson production), and is reabsorbed in the proton with a momentum $x-\xi$. During the reaction, a quadrimomentum t is transferred to the nucleon (Figure 1).

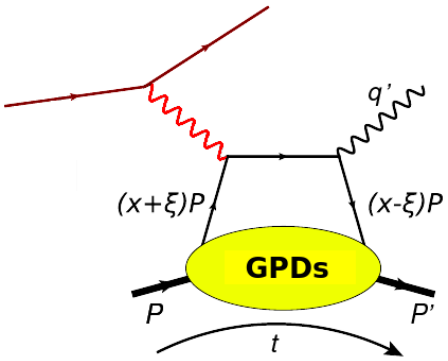

Figure 1: Feynman diagram of DVCS at lowest order.

We count four chiral-even GPDs (which do not involve quark-helicity flip), H, E, $\tilde{H}$, $\tilde{E}$, and as many chiral-odd GPDs (which involve quark-helicity flip). Those GPDs are functions of x, ξ, and t. The second moment in x of the sum of H and E for a given quark flavor gives the quark total angular momentum (this property is called the Ji sum rule [3]). As a consequence, the study of H and E are of first importance to understand the content of the proton in spin. COMPASS at CERN has the ability to study GPD H, and might have some potential to study GPD E.

2. The COMPASS experiment at CERN

2.1 COMPASS experimental setup

COMPASS (Common Muon Proton Apparatus for Structure and Spectroscopy) at CERN is a large acceptance magnetic spectrometer dedicated to the study of hadronic physics. It is installed on one of the Super-Proton-Synchrotron beam lines, and is able to receive beams of various types: protons, pions, and both positive and negative polarized muons (polarization $\simeq 80$ %).

The experimental setup is composed of two dipoles and of a large number of tracking detectors for charged particle reconstruction and momentum measurement. A ring imaging Cherenkov detector provides particle identification, and two electromagnetic or hadronic calorimeters provide

energy measurement. A more complete description of the detectors is provided in [4, 5]. Such an apparatus grants COMPASS with a wide kinematic range.

The experimental setup described above can be modified or completed to measure a specific process. Let us review the modifications that have been done for DVCS measurement.

2.2 Compass configuration for DVCS measurement

At COMPASS, the DVCS ($\mu p \to \mu p \gamma$) will be measured using the polarized muon beam ($\sim 4 \times 10^8\,\mu$ per 9.4 seconds long spill, repeated every 48 seconds, for μ^+). DVCS is a relatively low cross section process, so the luminosity will be enhanced with a 2.5 meter long liquid hydrogen target. In the DVCS kinematics, the photon is produced at forward angle, and the proton recoils at very large angle. To measure and identify the recoil proton, a 4-meter long Time-Of-Flight detector called CAMERA is surrounding the target. To extend the kinematic coverage of DVCS detection to the higher x_{Bj}, a large angle electromagnetic calorimeter has also been added. With such an apparatus, COMPASS can measure the DVCS process on a wide x_{Bj} range (from 0.005 to $\simeq 0.3$) with a Q^2 up to $\simeq 20\,\mathrm{GeV}^2$ (limited by integrated luminosity).

3. The COMPASS GPD program

Thanks to several advantageous features, which we are going to discuss, COMPASS has the ability to study both GPD H [6] and potentially GPD E. First, both μ^+ and μ^- beams are available at COMPASS (Sec. 2.1), each having one polarization direction. This feature is currently unique, and will provide useful additional information for the extraction of GPDs thanks to DVCS measurement (see Secs. 3.1 and 3.2). In addition to this, the x_{Bj} range covered by COMPASS ($0.005 < x_{Bj} < 0.3$) spans over the existing gap between the DVCS data from HERA in the gluon region ($x_{Bj} \leq 10^{-2}$) on the one hand, and the data from HERMES and Jefferson Lab in the valence region ($x_{Bj} \geq 0.1$). COMPASS is also a versatile detector, in this sense that it is able to measure simultaneously DVCS and several exclusive neutral meson channels, such as π^0, ρ^0, ϕ, ω.

3.1 Study of GPD H on hydrogen with recoil proton detection

The GPD H is studied with DVCS measurements on unpolarized hydrogen. The first proof of principle for the possibility to measure DVCS in COMPASS was brought by a 10-day long run test in 2009 with a reduced setup (40 cm liquid hydrogen target, short recoil proton calorimeter, no additional calorimetry).

3.1.1 Results from 2012 DVCS pilot run

In 2012, a four-week long pilot run has been recorded, with a mostly complete DVCS setup (full scale recoil proton detector, full luminosity, partially equipped large angle calorimeter). The analysis of this data is ongoing, but a milestone has already been reached by unfolding the distribution of DVCS signal. The main steps of this first part of the analysis are explained below.

The following elements are required for the first step of DVCS sample selection: vertices reconstructed with one beam track and one outgoing muon track, in the target volume; only one high energy photon (threshold: 4/5/10 GeV on large/medium/low angle calorimeter, respectively); and at least one track in the recoil proton detector, pointing towards the vertex.

This sample still contains a lot of combinatorial background. A very efficient way to clean this background is to compare the proton track reconstructed in the recoil detector with the "missing proton" quadrivector which can be deduced from the three other particles assuming our reaction is exclusive. In practice, we compare the differences of azimuthal angle ($\Delta\phi$) and of transverse momentum ($\Delta P_\perp$) between the reconstructed recoil proton and the "missing proton", which are both expected to be zero within resolution and radiative effects. We also reconstruct M_X^2, the missing mass of the system $\mathrm{H}(\mu,\mu'\gamma p)X$, which is also expected to be zero (within resolution and radiative effects). Tight cuts applied around the peaks of $\Delta\phi$, $\Delta P_\perp$, and M_X^2 distributions rule out most of the combinatorial background.

After this step, there remains in the exclusive photon sample a significant contamination which source is the production of π^0, where one of the photon mimics the high energy photon. In this event, there are two possibilities: the other photon can be detected or not. If the other photon is detected ("visible leaking π^0"), the contamination is clearly evidenced by the reconstruction of the two photon invariant mass where one of the photon is the high energy photon (Figure 2). This contribution is ultimately removed by a cut of $\pm 20\,\mathrm{MeV/c^2}$ around the PDG π^0 mass. If the other

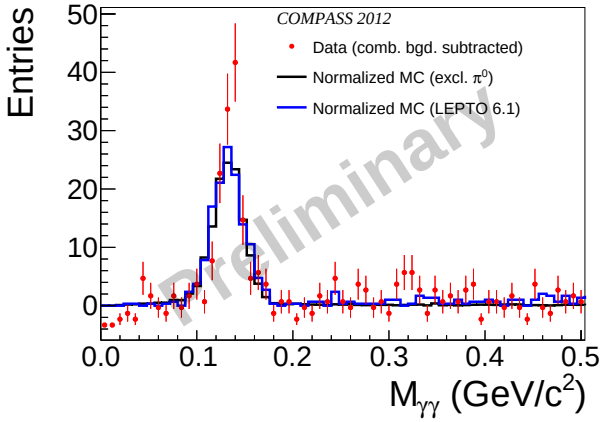

Figure 2: Two photon invariant mass in the exclusive single photon sample. There is a visible π^0 contribution in the data (red dots), which can been compared either to exclusive π^0 Monte Carlo simulation (HEPGEN/π^0, black histogram), or to semi-inclusive π^0 Monte Carlo simulation (LEPTO, blue histogram).

photon is not detected, Monte Carlo simulations are required to evaluate this background. There are two Monte-Carlo samples available, one with exclusive π^0 (HEPGEN/π^0), one with semi inclusive π^0 (LEPTO). Those samples are normalized to the data with respect to the number of π^0 (see again Figure 2) in the visible leaking π^0 peak. The number of "invisible" π^0 contributing to the exclusive photon sample can be retrieved knowing the number of true Monte-Carlo π^0 corresponding to the number of reconstructed π^0 in the peak. Since we do not have yet a perfect handle on the respective normalizations of the LEPTO and HEPGEN/π^0 Monte-Carlo simulations with respect to each other, we prefer for the moment to evaluate the contamination from the two Monte-Carlo samples separately; the contamination from pure semi-inclusive π^0 and pure exclusive π^0 giving respectively the upper and lower limits for the invisible π^0 contribution to the exclusive photon sample.

The final exclusive photon sample is displayed in Figure 3, as a function of $\phi_{\gamma^*\gamma}$, the azimuthal

angle between the leptonic plane (defined by the incident and scattered lepton) and the hadronic plane (defined by the virtual and real photon), for the 3 following bins in x_{Bj}: $0.005 < x_{Bj} < 0.01$; $0.01 < x_{Bj} < 0.03$; $0.03 < x_{Bj} < 0.27$. This binning allows to "isolate" the Bethe-Heitler

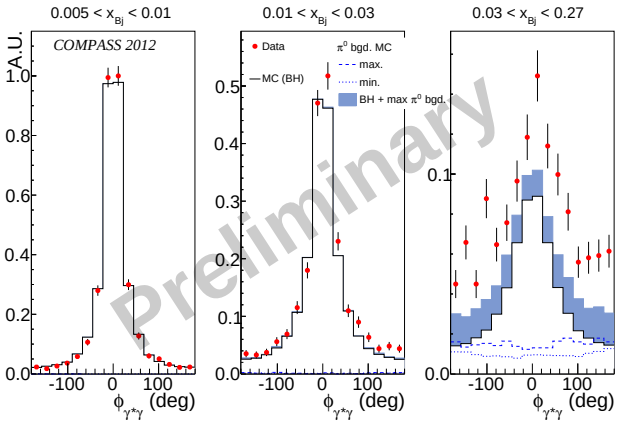

Figure 3: The exclusive single photon events obtained in the 2012 sample as a function of $\phi_{\gamma^*\gamma}$ (red dots) compared to the Bethe-Heitler estimation (black histogram) and the π^0 contamination estimated by LEPTO and HEPGEN. The visible π^0 background has been subtracted from these data.

contribution at low x_{Bj}. The Bethe-Heitler process shares the same final state as DVCS (therefore it interferes with it), but the photon is radiated by the incident or the scattered lepton instead of the proton. The amplitude of the Bethe-Heitler process can be calculated with very good accuracy, and on Figure 3, the Monte-Carlo estimation (black histogram) only includes Bethe-Heitler.

In the lower x_{Bj} bin, where the DVCS contribution is negligible, the $\phi_{\gamma^*\gamma}$ distribution for the data (red dots) agrees remarkably well in shape with the Bethe-Heitler estimation by Monte-Carlo. For the reason that we do not have yet a perfect handle on the Monte Carlo absolute normalization, we have normalized the Monte-Carlo sample to the data on this bin, and this normalization factor has been applied on the other x_{Bj} bins. In the larger x_{Bj} bin, there is a significant excess of events, beyond the pure Bethe-Heitler contribution (black histogram), and beyond the maximal estimation for invisible π^0 contribution (blue solid histogram). This excess of events can be interpreted as DVCS. The analysis of the t-slope of the DVCS cross section with this statistics is ongoing.

3.1.2 Projection for full DVCS run in 2016-2017

The full DVCS run will occur in 2016 and 2017 [6]. Interesting information will come from the $\mu p \to \mu p \gamma$ cross sections measurements with both muon charge states ($d\sigma(\mu^{+,\rightarrow})$ and $d\sigma(\mu^{-,\leftarrow})$) both from their sum $\mathscr{S}_{CS,U}$ and their difference $\mathscr{D}_{CS,U}$.

The DVCS cross section can be isolated from $\mathscr{S}_{CS,U}$. Its t-dependence, expected to be in $\exp(-Bt)$, provides the transverse radius of the proton $r_\perp$ at the measured x_{Bj}, knowing that $\langle r_\perp^2(x_{Bj})\rangle \simeq 2B(x_{Bj})$. The transverse radius is the transverse spatial extension of the partons with a momentum fraction x_{Bj}. The t-slope parameter B has been measured at HERA at $x_{Bj} < 0.01$ (square and triangles on Fig. 4). In this region, B is measured to be constant. In the x_{Bj} range covered by COMPASS, the proton size is expected to shrink (solid and dashed lines on Fig. 4), and the projected COMPASS uncertainties with two years of data (circles on Fig. 4) should be able to determine the x_{Bj}-slope, α' of this shrink.

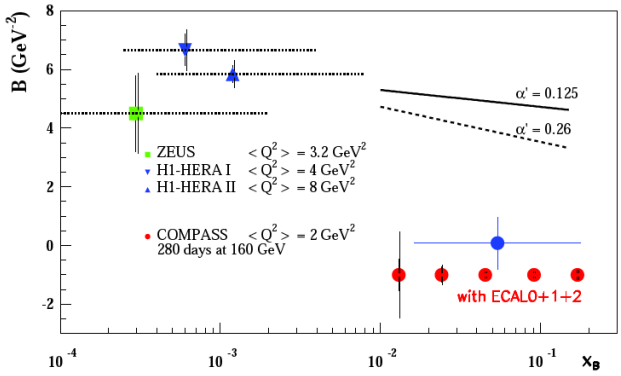

Figure 4: t-slope parameter as a function of x_{Bj} measured by HERA (square and triangles) [7, 8, 9], and projected statistical uncertainty with two years of data at COMPASS (circles).

The study of the $\phi_{\gamma^*\gamma}$ modulation of the Bethe-Heitler-DVCS interference term in $\mathscr{S}_{CS,U}$ and $\mathscr{D}_{CS,U}$ allow to isolate their first $\phi_{\gamma^*\gamma}$ moment (respectively $s_1^{Int}\sin(\phi_{\gamma^*\gamma})$ and $c_1^{Int}\cos(\phi_{\gamma^*\gamma})$), which depend respectively on the imaginary part and real part of $F_1 \times \mathscr{H}$. ($\mathscr{H}$ being the observable of the GPD H, called Compton form factor). An illustration of the expected experimental precision

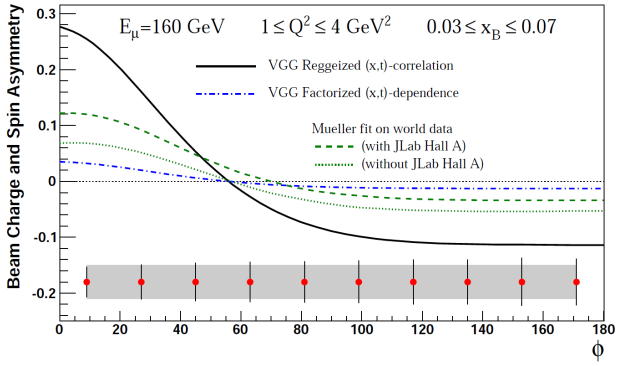

Figure 5: Projected statistical accuracy for a measurement of the $\phi_{\gamma^*\gamma}$ dependence of the beam charge and spin asymmetry with 280 days (global efficiency $\varepsilon = 0.10$) of data at COMPASS (circles), for the 2-dimensional bin $0.03 < x_{Bj} < 0.07$ and $1.0 < Q^2 < 4.0\,\mathrm{GeV}^2/c^4$ is shown. Predictions are calculated using the VGG model [10, 11, 12, 13]. The black (solid) and blue (dash-dotted) curves correspond to two different variants of the VGG model. The green curves show predictions based on the first fit of world data [14] including the old JLab Hall A data (dashed line) or not (dotted line).

for the $\phi_{\gamma^*\gamma}$ modulation of the beam spin-charge asymmetry is provided on Figure 5. Predictions from VGG model [10, 11, 12, 13] and the first fit of world data available before 2015 [14] are also displayed.

3.2 Study of GPD E with transversely polarized proton target

The measurements of DVCS and exclusive meson production on polarized hydrogen allow to study the GPD E, which allows for nucleon spin flip. Results of exclusive vector meson production off a transversely polarized proton target have already been published or released by COMPASS.

A very challenging project of DVCS measurement on a polarized proton target is also being investigated.

3.2.1 Results of exclusive vector meson production on transversely polarized proton target (without recoil proton detection)

The exclusive production of ρ^0 and ω mesons on a transversely polarized hydrogen target (without recoil detection) has been performed with muon data recorded at COMPASS between 2007 and 2010. Eight target spin asymmetries, depending on ϕ and ϕ_S (ϕ_S being the angle between muon scattering plane and proton polarization) have been extracted [15, 16]. The most statistically accurate of these quantities are displayed on Figure 6, as a function of x_{Bj}, Q^2 and p_T^2, for the ρ^0 (left panel) and the ω (right panel).

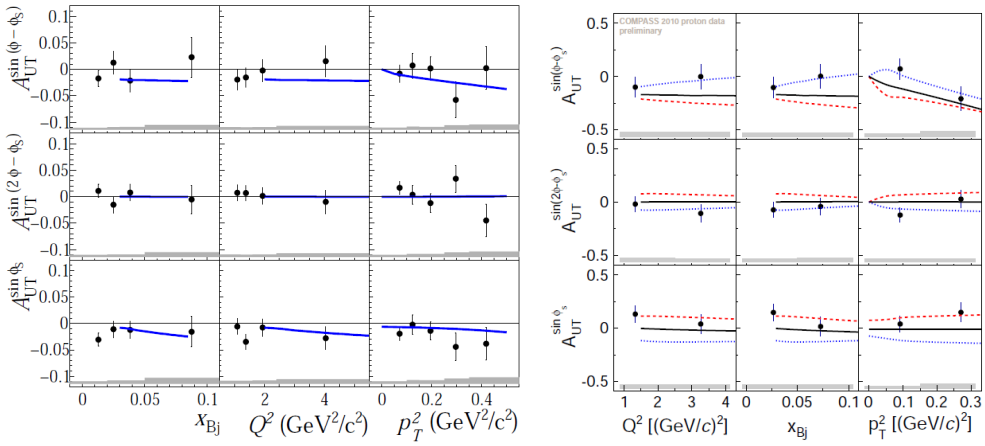

Figure 6: Target spin asymmetries on $\mu p^{\uparrow\downarrow} \to \mu p \rho^0$ (left) and $\mu p^{\uparrow\downarrow} \to \mu p \omega$ (right) measured at COMPASS [15, 16] as a function of x_{Bj}, Q^2 and p_T^2. Top, middle, bottom panels show $\sin(\phi - \phi_S)$, $\sin(2\phi - \phi_S)$, $\sin\phi_S$ contributions, respectively. The solid curves represent a GPD model calculation from Goloskokov and Kroll [17]. On the right panel, blue and red dashed curves represent calculations where the GPDs are embedded in pion pole contributions (with negative and positive $\omega - \pi$ form factor, respctively) [18].

Those asymmetries have been successfully interpreted in terms of GPDs for the ρ^0. The $\sin(\phi - \phi_S)$ term is measured to be rather small, and is in good agreement with the GPD model from Goloskokov and Kroll [17] (blue curves on Figure 6). In the framework of GPDs, this term depends on GPD E at leading order. The gluon and the sea quark contributions canceling, the process amplitude depends on the valence quark contribution. Because of the ρ^0 quark content, and as E^u and E^d are expected to be of same order of magnitude, the $\sin(\phi - \phi_S)$ asymmetry is expected to be small. Using a similar argument for the ω, this term would be expected to be much larger (see next paragraph). The $\sin(2\phi - \phi_S)$ asymmetry is measured to be almost zero, and the $\sin\phi_S$ asymmetry is measured to be significantly non-zero; they are also in good agreement with the GPD model. Considering the combinations of GPDs those two terms respectively depend, one may deduce that the chiral-odd GPD H_T should not be small.

As we already mentioned in the previous paragraph, the $\sin(\phi - \phi_S)$ term would be expected to be consequent for ω production. The measurements are actually compatible with a model where GPD amplitudes are embedded with pion pole contributions (dashed and dotted curves on right

panel of Figure 6, from Goloskokov and Kroll [18]). However, those measurements do not allow to disambiguate the sign of $\omega - \pi$ form factor.

3.2.2 Future perspective of DVCS on transversely polarized proton target (with recoil proton detection)

In the future, COMPASS might also be able to measure DVCS on a transversely polarized target, with recoil proton detection. The measurement of first moment in $\phi - \phi_s$ of the charge spin cross section difference on a transversely polarized target, $\mathscr{D}_{CS,T}$, provides access to both Compton form factors $\mathscr{H}$ and $\mathscr{E}$ on the same footing. This challenging prospect is still under investigation,

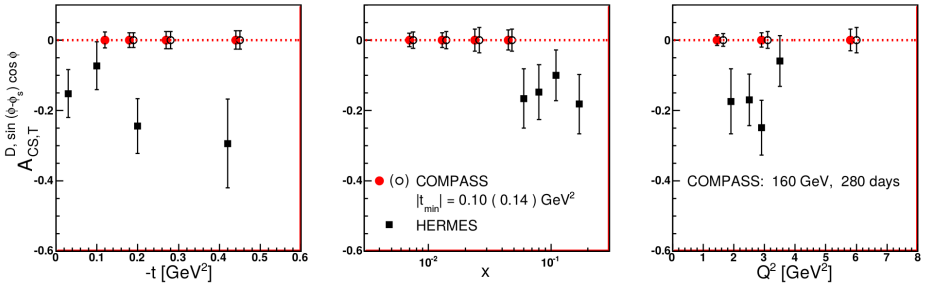

Figure 7: Expected statistical accuracy of $A_{CS,T}^{D,\sin(\phi-\phi_S)\cos\phi}$ as a function of t, x_{Bj} and Q^2 from a measurement in 280 days ($\varepsilon = 0.10$), using a 160 GeV muon beam and a 1.2 m long transversely polarized hydrogen target. Solid and open circles correspond to the simulations for the two hypothetical configurations of the target region. Also shown is the asymmetry $A_{UT}^{\sin(\phi-\phi_S)\cos\phi}$ measured at HERMES [19] with its statistical errors.

as it is currently technically limited by the combination of a transversely polarized target (which, by order, is surrounded by a magnet) with recoil proton detection. The additional material around the target translates into a hard cut in the lower values of the quadrimomentum t, as only protons with a higher momentum are able to cross this material. On Figure 7, two scenarios are evaluated, which depend on the technical progress made for polarized targets with thin magnets: an optimistic one where the minimal t-value imposed by the material thickness is $0.10\,\mathrm{GeV/c^2}$ (red dots on Figure 7), and a more realistic one where this value is $0.14\,\mathrm{GeV/c^2}$ (hollow dots on Figure 7). Even in the worst case, COMPASS could improve by better than a factor 2 the statistical accuracy on this quantity compared to its previous measurement by HERMES [19] with two years of data [6].

4. Summary

The study of the GPDs is one of the hot topics in the structure of the nucleon. The COMPASS experiment, with its unique features (Sec. 3), offers a very promising GPD program. The existing results (Sections 3.1.1 and 3.2.1) are very encouraging to go forward the forthcoming full DVCS run (2016-2017), which will provide a good accuracy for the measurement of several observables of interest (proton size, Compton form factor $\mathscr{H}$, see Section 3.1.2). The possibility to measure DVCS on transversely polarized target at COMPASS, though being a technical challenge, is also being investigated (Section 3.2.2), and would allow to study Compton form factor $\mathscr{E}$.

5. Acknowledgments

We would like to acknowledge the P2IO Excellence Laboratory for its financial support.

References

[1] D. Müller, D. Robaschik, B. Geyer, F.-M. Dittes and J. Hořejši, Fortsch. Phys. **42** (1994) 101 [hep-ph/9812448].

[2] A. V. Radyushkin, Phys. Rev. D **56** (1997) 5524 [hep-ph/9704207].

[3] X. D. Ji, Phys. Rev. Lett. **78** (1997) 610 [hep-ph/9603249].

[4] P. Abbon *et al.* [COMPASS Collaboration], Nucl. Instrum. Meth. A **577** (2007) 455 [hep-ex/0703049].

[5] P. Abbon *et al.* [COMPASS Collaboration], Nucl. Instrum. Meth. A **779** (2015) 69 [arXiv:1410.1797 [physics.ins-det]].

[6] F. Gautheron *et al.* [COMPASS Collaboration], CERN-SPSC-2010-014.

[7] F. D. Aaron *et al.* [H1 Collaboration], Phys. Lett. B **659** (2008) 796 [arXiv:0709.4114 [hep-ex]].

[8] A. Aktas *et al.* [H1 Collaboration], Eur. Phys. J. C **44** (2005) 1 [hep-ex/0505061].

[9] S. Chekanov *et al.* [ZEUS Collaboration], JHEP **0905** (2009) 108 [arXiv:0812.2517 [hep-ex]].

[10] M. Vanderhaeghen, P. A. M. Guichon and M. Guidal, Phys. Rev. Lett. **80** (1998) 5064.

[11] M. Vanderhaeghen, P. A. M. Guichon and M. Guidal, Phys. Rev. D **60** (1999) 094017 [hep-ph/9905372].

[12] K. Goeke, M. V. Polyakov and M. Vanderhaeghen, Prog. Part. Nucl. Phys. **47** (2001) 401 [hep-ph/0106012].

[13] M. Guidal, M. V. Polyakov, A. V. Radyushkin and M. Vanderhaeghen, Phys. Rev. D **72** (2005) 054013 [hep-ph/0410251].

[14] K. Kumerički and D. Mueller, Nucl. Phys. B **841** (2010) 1 [arXiv:0904.0458 [hep-ph]].

[15] C. Adolph *et al.* [COMPASS Collaboration], Phys. Lett. B **731** (2014) 19 [arXiv:1310.1454 [hep-ex]].

[16] C. Adolph *et al.* [COMPASS Collaboration], Nucl. Phys. B **865** (2012) 1 [arXiv:1207.4301 [hep-ex]].

[17] S. V. Goloskokov and P. Kroll, Eur. Phys. J. C **74** (2014) 2725 [arXiv:1310.1472 [hep-ph]].

[18] S. V. Goloskokov and P. Kroll, Eur. Phys. J. A **50** (2014) 9, 146 [arXiv:1407.1141 [hep-ph]].

[19] A. Airapetian *et al.* [HERMES Collaboration], JHEP **0806** (2008) 066 [arXiv:0802.2499 [hep-ex]].